

Absolute differential cross sections for very-small-angle elastic scattering in He + He collisions at keV energies

D. E. Nitz,* R. S. Gao, L. K. Johnson, K. A. Smith, and R. F. Stebbings

Space Physics and Astronomy Department and the Rice Quantum Institute, Rice University,
Houston, Texas 77251

(Received 26 November 1986)

Absolute differential cross sections for He + He elastic scattering at laboratory angles in the range 0.018° – 0.5° have been measured for projectile energies of 0.5, 1.5, and 5.0 keV. The experiment employs a position-sensitive detector for determining the angular distribution of scattered particles. The differential cross sections exhibit a transition from classical to quantum behavior within the range of angles studied, and excellent agreement is observed with partial-wave-theory calculations using phase shifts derived from the He-He interaction potentials of Ceperley and Partridge [J. Chem. Phys. **84**, 820 (1986)] and Foreman, Rol, and Coffin [J. Chem. Phys. **61**, 1658 (1974)].

INTRODUCTION

Recently, Newman *et al.*¹ reported measurements of absolute differential cross sections for scattering of keV-energy helium atoms by atomic and molecular targets at laboratory angles in the range of 0.13° – 5.0° . Their experiment made use of a position-sensitive detector (PSD), which permitted the accumulation of high-resolution data simultaneously at all angles. The present paper describes the extension of the He + He measurements to the next lower decade of scattering angles, covering a range 0.018° – 0.5° . The study of elastic scattering at such small angles is interesting from a fundamental point of view because it encompasses the transition from classical to quantum behavior and also because these collisions probe the lower repulsive wall of the He-He potential, a region that has been the subject of recent discussion in the literature.^{2,3} Whereas fast-beam experiments have previously probed the potential at internuclear separations smaller than about 1.6 Å, the extension of differential cross-section measurements to smaller angles increases this range outward to provide a region of overlap with results obtained by thermal energy techniques.

Since the scattering in the present experiment corresponds to minute deflections at relatively large impact parameters, it is amenable to a straightforward partial-wave analysis using semiclassical phase shifts.^{4,5} We have carried out these calculations to compare the experimental results with differential cross sections derived from recently proposed forms of the He-He interaction potential.

APPARATUS

A schematic of the apparatus appears in Fig. 1. A momentum-analyzed beam of He⁺ ions is partially neutralized upon passage through a helium-filled charge transfer cell (CTC). Ions remaining in the beam are removed by deflection plates DP1, while the neutral atoms continue on to the target cell (TC). The beam is collimated to a divergence of less than 0.003° by the exit aperture of the CTC and the entrance aperture of the TC, which

are 20 and 30 μm in diameter, respectively, and are separated by 49 cm. The symmetric nature of the charge-transfer process and the kinematics associated with the narrow collimation ensure that virtually all the helium atoms entering the target cell are in the ground state.¹ The target cell is 3.65 mm in length and has an exit aperture 300 μm in diameter. Deflection plates DP2 at the exit are used to remove any charged collision products from the beam (and to sweep ion beams employed in diagnostic studies of the detector).

A PSD with an active region 2.5 cm in diameter is situated 109 cm beyond the target cell. This geometry permits a maximum observable scattering angle of about 0.7° . An LSI 11/2 microcomputer is used to monitor the output of the PSD electronics and register the arrival coordinates of each detected particle in a 90×90 array whose bin dimension may be varied according to the angular resolution desired. For measurements below 0.2° , the bin dimension used corresponds to a distance of 68.7 μm on the PSD surface, which amounts to an angular step size of 0.0037° per bin. At larger angles, the bin size is set to be 2 or 4 times larger. Absolute calibration of the PSD is obtained by observing the shadow of a grid of known dimensions placed directly in front of the detector. The characteristics of the detector and its application to scattering experiments have been described in detail by Newman *et al.*¹ and Gao *et al.*⁶

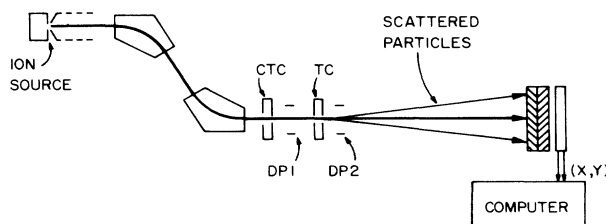


FIG. 1. Schematic of the apparatus (relative distances not drawn to scale).

Background pressure in the chambers containing the gas cells and the detector is maintained at approximately 3×10^{-7} Torr. At a typical target cell pressure of 5 mTorr, the density-length product of the target gas exceeds that of the background gas by roughly a factor of 70. At this target cell pressure, the scattered fraction of the beam is only 5%, and multiple collision effects are negligible.

MEASURED QUANTITIES

The differential cross section is related to measurable parameters under thin-target conditions by the expression

$$\frac{d\sigma}{d\Omega}(\theta) = \frac{\Delta S(\theta)}{S \int n(l) dl \Delta\Omega}, \quad (1)$$

where S is the primary beam flux in particles per second, $\Delta S(\theta)$ is the flux scattered at angle θ into a solid angle $\Delta\Omega$ steradians, $n(l)$ is the target density, and dz is an element of path length of the beam through the target gas.

As demonstrated by Newman *et al.*,¹ for a target cell with a length-to-exit-aperture ratio of 12.2 the integrated target density is accurately given by the product nL , where L is the physical length of the target cell and n is obtained from a measurement of target cell pressure using an MKS Baratron corrected for thermal transpiration.^{1,7}

Measurement of the scattered flux, $\Delta S(\theta)$, requires that one distinguish between counts due to scattering in the target cell and background counts arising from other sources such as scattering from the background gas, scattering from the apertures, and random detector noise. This is accomplished by accumulating data with and without gas in the target cell. $\Delta S(\theta)$ is given by the difference between these two signals as long as the presence of the target gas has a negligible effect on the backgrounds. Measurements at several values of target cell pressure yielded essentially identical differential cross-section data. One concludes, therefore, that the presence of target gas did not have a significant effect on background count rates.

Data are typically accumulated until the statistical uncertainty in the signal at a representative angle is less than 10%. At primary beam count rates which range from ten per second to several hundred per second, this takes between 20 minutes and a few hours.

Absolute determination of $\Delta S(\theta)$ would require knowledge of the detection efficiency for scattered particles. However, since the cross section depends on the ratio $\Delta S(\theta)/S$, this efficiency need not be known if one can ensure that the scattered particles are detected with the same efficiency as primary beam particles. While the PSD efficiency is, in general, somewhat dependent on the local count rate, it is possible to equalize the detection efficiencies for primary and scattered particles to within a few percent by careful selection of the PSD operating voltage. This involves measurement of the relative detection efficiency as a function of PSD operating voltage for both diffuse and localized He^+ beams of appropriate intensity, a procedure we carry out each time cross sections are measured.^{1,6}

Since the dark current of the detector is negligible in

comparison with the primary beam flux, the gas-out data provide a measure of the primary flux S . The statistical center of the gas-out distribution is computed to establish the coordinate origin for measurement of scattering angles.

Cross sections are calculated by organizing the 90×90 data array into concentric rings whose width (equal to two array bins) is chosen subject to the competing demands of good angular resolution and an acceptable rate of data accumulation per ring. Counts registered in the i th ring are assigned to the angle θ_i which is the average of the angles corresponding to the inner and outer radii of the ring. The angles θ_i are known to within $\pm(0.03\theta_i + 0.002^\circ)$ degrees, reflecting the uncertainties in PSD calibration, the distance from target cell to detector, and location of beam center. However, one is interested not only in the value of θ_i , but in the range $\Delta\theta$ of physical scattering angles that contribute to the signal at θ_i due to various properties of the apparatus that degrade the resolution. The most important of these properties in the present experiment (and the associated values of $\Delta\theta$) are the nonzero angular width of the primary beam (0.008°), the discrete nature of the analysis rings (0.008° – 0.03° , depending on the bin size used), and electronic errors in the detector's position-encoding circuitry ($\Delta\theta$ variable). While the first two factors are straightforward, the third has some subtle consequences to the nature of the PSD output pulse-height spectrum.

The PSD spatial resolution is related to the size of the electron pulse impinging on the resistive anode. This phenomenon has been studied with use of a single channel analyzer (SCA) to record the contributions to the electronic image of the primary beam from different portions of the pulse-height spectrum. In general, we find that the largest pulses provide good signal-to-noise ratio for the position-encoding electronics and result in accurate position data, but the smallest pulses (amounting to a few percent of the total counts) may be registered as much as $1000 \mu\text{m}$ outside the geometrically-limited impact region. The details of the distribution depend on operating conditions: the problem is accentuated by high local count rates and by low PSD operating voltage, both of which increase the relative number of small output pulses. Under conditions appropriate to the collection of data for 0.5 keV collisions, we find that 95% of the counts are recorded with an error less than 0.016° , 3% with an error between 0.016° and 0.032° , and the remaining 2% are distributed out to 0.05° . The relatively inaccurate position assignment for so few particles clearly does not constitute a serious loss of angular resolution *per se*; it does, however, interfere with measurement of the scattered signal at the smallest angles ($\theta < 0.05^\circ$), where spurious primary beam counts increase the apparent diameter of the primary beam. These counts can be eliminated (and the angular resolution enhanced) by using the SCA to reject the small pulses, but one cannot obtain *absolute* cross sections using the SCA since the pulse-height distributions for primary and scattered particles are not the same, resulting in different detection efficiencies for primary and scattered particles when a limited range of the pulse-height spectrum is sampled. Therefore, our procedure for measuring

cross sections below 0.05° is to obtain relative data using the SCA, and to then normalize these by a least-squares procedure to the absolute data at angles greater than 0.05° , where the effects of the spurious primary beam counts are negligible. In principle, the resolution of the experiment is also influenced by the length of the target cell, the beam

divergence, and thermal motion of the (room temperature) target, but these factors are not significant relative to the beam size, ring size, and the position-encoding errors.

RESULTS

Cross sections have been determined at laboratory-frame collision energies of 0.5, 1.5, and 5.0 keV, and the

TABLE I. Laboratory frame differential cross sections, $d\sigma(\theta)/d\Omega$, for He + He collisions, where E is the projectile energy. Uncertainty in θ is $\pm(0.03\theta + 0.002^\circ)$. Numbers in square brackets represent power of ten.

| θ (deg) | $\frac{d\sigma(\theta)}{d\Omega}$ ($\text{\AA}^2/\text{steradian}$) | | |
|-------------------|---|----------------|----------------|
| | $E = 0.5$ keV | $E = 1.5$ keV | $E = 5.0$ keV |
| 0.018 | 1.84±0.28 [06] | 2.98±0.36 [06] | 4.19±0.44 [06] |
| 0.026 | 1.60±0.23 [06] | 2.76±0.31 [06] | 2.68±0.29 [06] |
| 0.033 | 1.40±0.19 [06] | 2.05±0.23 [06] | 1.32±0.15 [06] |
| 0.040 | 1.21±0.16 [06] | 1.72±0.20 [06] | 8.54±1.02 [05] |
| 0.048 | 9.76±1.37 [05] | 1.19±0.14 [06] | 4.12±0.59 [05] |
| 0.055 | 8.54±0.69 [05] | 7.32±0.59 [05] | 3.50±0.30 [05] |
| 0.062 | 7.12±0.58 [05] | 5.03±0.41 [05] | 2.76±0.24 [05] |
| 0.070 | 5.58±0.45 [05] | 3.27±0.27 [05] | 2.45±0.21 [05] |
| 0.077 | 4.22±0.32 [05] | 2.13±0.18 [05] | 1.90±0.17 [05] |
| 0.085 | 3.31±0.27 [05] | 1.51±0.13 [05] | 1.60±0.14 [05] |
| 0.092 | 2.54±0.21 [05] | 1.26±0.11 [05] | 1.35±0.12 [05] |
| 0.099 | 1.84±0.15 [05] | 1.02±0.09 [05] | 1.14±0.10 [05] |
| 0.107 | 1.37±0.11 [05] | 9.11±0.80 [04] | 9.48±0.87 [04] |
| 0.114 | 9.40±0.76 [04] | 9.18±0.80 [04] | 8.14±0.63 [04] |
| 0.121 | 7.59±0.62 [04] | 8.28±0.72 [04] | 8.03±0.74 [04] |
| 0.129 | 5.83±0.47 [04] | 7.20±0.63 [04] | 6.62±0.63 [04] |
| 0.136 | 5.01±0.42 [04] | 6.76±0.59 [04] | 5.94±0.58 [04] |
| 0.143 | 4.86±0.40 [04] | 5.39±0.48 [04] | 5.34±0.56 [04] |
| 0.151 | 4.30±0.37 [04] | 4.96±0.45 [04] | 5.04±0.52 [04] |
| 0.158 | 4.55±0.39 [04] | 4.55±0.42 [04] | 4.75±0.48 [04] |
| 0.165 | 4.02±0.36 [04] | 4.19±0.39 [04] | 4.41±0.46 [04] |
| 0.173 | 4.08±0.36 [04] | 3.81±0.38 [04] | 3.54±0.40 [04] |
| 0.180 | 4.50±0.38 [04] | 3.51±0.37 [04] | 3.19±0.36 [04] |
| 0.187 | 4.19±0.38 [04] | 2.99±0.35 [04] | 3.06±0.38 [04] |
| 0.195 | 3.96±0.38 [04] | 2.78±0.35 [04] | 2.63±0.41 [04] |
| 0.202 | 3.36±0.38 [04] | 2.79±0.39 [04] | 2.72±0.43 [04] |
| 0.206 | | 2.56±0.20 [04] | |
| 0.213 | 3.03±0.25 [04] | | 2.18±0.19 [04] |
| 0.228 | 2.47±0.20 [04] | | |
| 0.243 | 2.10±0.17 [04] | | 1.63±0.14 [04] |
| 0.252 | | 1.61±0.13 [04] | |
| 0.257 | 1.85±0.15 [04] | | |
| 0.272 | 1.62±0.13 [04] | | 1.16±0.11 [04] |
| 0.287 | 1.55±0.13 [04] | | |
| 0.298 | | 1.17±0.09 [04] | |
| 0.301 | 1.43±0.12 [04] | | 8.75±0.83 [03] |
| 0.316 | 1.37±0.11 [04] | | |
| 0.331 | 1.15±0.09 [04] | | 6.08±0.62 [03] |
| 0.344 | 1.05±0.09 [04] | 8.53±0.68 [03] | |
| 0.360 | 8.87±0.72 [03] | | 5.64±0.56 [03] |
| 0.375 | 8.33±0.68 [03] | | |
| 0.390 | 8.26±0.68 [03] | 6.79±0.54 [03] | |
| 0.404 | 6.88±0.58 [03] | | |
| 0.419 | 6.48±0.56 [03] | | |
| 0.434 | 6.59±0.56 [03] | 5.01±0.40 [03] | |
| 0.448 | 5.71±0.50 [03] | | |
| 0.463 | 5.30±0.48 [03] | | |
| 0.481 | | 4.19±0.34 [03] | |

TABLE II. Experimental uncertainties.

| Experimental quantity | Uncertainty contributed to $d\sigma(\theta)/d\Omega$ |
|---|--|
| Scattered signal, $\Delta S(\theta)$ | |
| counting statistics | 3–15% |
| PSD operating point | 4% |
| Primary beam flux S | 3% |
| Density n | |
| Pressure measurement and drift | 2% |
| Thermal transpiration correction | 2% |
| Target cell length L | 2% |
| Solid Angle $\Delta\Omega$ | |
| PSD calibration | 4% |
| TC-PSD distance | 2% |
| Normalization of data for $\theta < 0.05^\circ$ | 5% |

results are given in Table I. Factors which contribute to the experimental uncertainties are summarized in Table II.

The majority of the experimental effort has been devoted to the 0.5-keV case since, for a fixed range of scattering angles, it probes the largest values of internuclear separation. These data are plotted in Fig. 2 together with the data of Newman *et al.*,¹ which were obtained independently in this laboratory with a different apparatus and PSD. The consistency of the two sets of measurements is evident. Previous results for small-angle He + He scattering were reported by Leonas and Sermyagin,⁵ who measured relative differential cross sections at a resolution roughly an order of magnitude lower than that of the present experiment.

The behavior of the cross section below 0.2° is of particular interest. Whereas the classical differential cross section rises monotonically and diverges as θ approaches 0, the actual quantum behavior exhibits an undulating structure superimposed on the classical cross section and a lev-

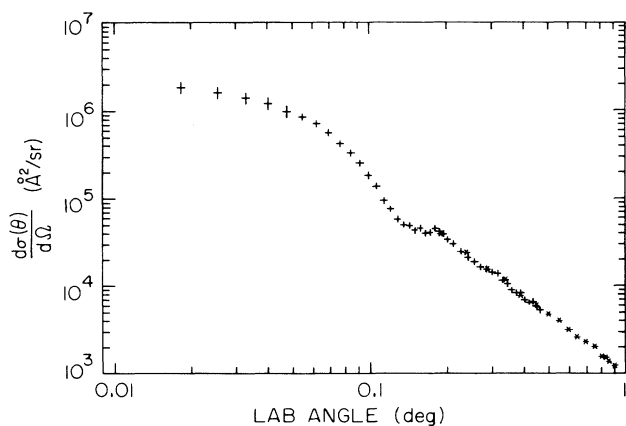


FIG. 2. Differential cross sections for He + He scattering at a projectile energy of 0.5 keV. +, present results; *, Newman *et al.* (Ref. 11).

eling off which varies as $e^{-c\theta^2}$ at small angles. Such behavior was predicted theoretically for model potentials^{8–10} and observed in thermal energy alkali-metal–mercury and alkali-metal–rare-gas collisions¹¹ in the early 1960's. It is referred to as the forward diffraction peak and is understood as arising from interference over a broad range of impact parameters associated with weak deflections from the tail of the potential.^{12,13} This contrasts with the behavior of rainbow or glory scattering, which are associated with a few particular impact parameters. When observed as a function of energy, a given undulation feature (the first minimum, for example) behaves analogously to optical diffraction from a disk, moving to smaller angles as the de Broglie wavelength decreases. Beier⁴ has utilized this analogy to relate the undulation characteristics to potential parameters in the case of a screened Coulomb interaction.

Depending on the collision energy and the potentials involved, the diffraction peak can be characteristic of either the attractive or the repulsive part of the potential. Partial-wave calculations indicate that the influence of the weak He-He van der Waals attraction is negligible in the present experiment.

The differential cross section is expressed quantum mechanically as the square of a complex scattering amplitude $f(\phi)$ which is given by the partial-wave summation formula

$$f(\phi) = \frac{1}{2ik} \sum_{l=0}^{\infty} (2l+1) P_l(\cos\phi) (e^{2i\delta_l} - 1), \quad (2)$$

where ϕ is the scattering angle in the center-of-mass frame, k is the wave number, δ_l is the phase shift of the l th partial wave, and $P_l(\cos\phi)$ is the l th Legendre polynomial. We have calculated cross sections from Eq. (2), using phase shifts derived from various proposed forms of the He-He interaction potential, for comparison with the experimental cross sections. Details of the computations are outlined in the Appendix.

Heretofore, information about the He-He interaction has been pieced together from a diverse combination of scattering experiments, dilute-gas transport experiments,

and theory.¹⁴ Recent attention in the literature has focused on the lower repulsive wall at internuclear separations less than 1.8 Å, where the potential rises above the 0.1-eV level. In this region the results of high-temperature transport experiments¹⁵ point to a more steeply rising potential than do scattering measurements of integral cross sections.^{2,16} Of the many potentials which could be investigated, two analytic forms which provide a convenient characterization of this situation are the potentials proposed by Aziz *et al.*¹⁷ and by Ceperley and Partridge.¹⁸ The potential of Aziz *et al.* has an attractive well consistent with a large body of thermal energy data and a steep repulsive wall consistent with the high-temperature (2500 K) measurements of thermal conductivity by Jody *et al.*¹⁹ Ceperley and Partridge have proposed a composite potential based on *ab initio* quantum Monte Carlo calculations and an extrapolation to larger r . This potential follows Aziz *et al.* for $r > 1.828$ Å, but at smaller r it agrees more closely with results of Feltgen *et al.*² and Foreman *et al.*,¹⁶ who obtained potentials by inverting integral cross-section data. This information is presented graphically in Fig. 3.

Theoretical differential cross sections for these potentials (transformed to the lab frame) are plotted in Fig. 4(a) along with the 0.5-keV experimental results. In general, the agreement in both shape and magnitude of the cross sections is excellent, and we emphasize that this comparison includes no adjustable parameters. At angles less than 0.1°, the predictions are almost identical (since the potentials are identical for $r > 1.828$ Å) and lie within the experimental uncertainty of the data. At angles greater than 0.1°, the steeper nature of the Aziz *et al.* potential yields larger amplitude undulations than are observed experimentally and slightly lower values of the cross section. The prediction based on the Ceperley and Partridge potential lies within the uncertainty of the data throughout almost the entire angular range of the experiment. We have also carried out calculations using the exponential potential of Foreman *et al.* extrapolated to larger r . The results exhibit a slightly weaker undulation between 0.1° and

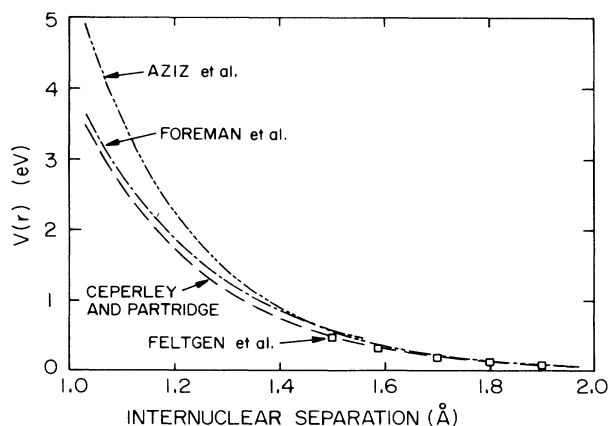


FIG. 3. He-He interaction potentials. □, Feltgen *et al.* (Ref. 2); — · — · —, Foreman *et al.* (Ref. 16); — — —, Aziz *et al.* (Ref. 17); — — —, Ceperley and Partridge (Ref. 18).

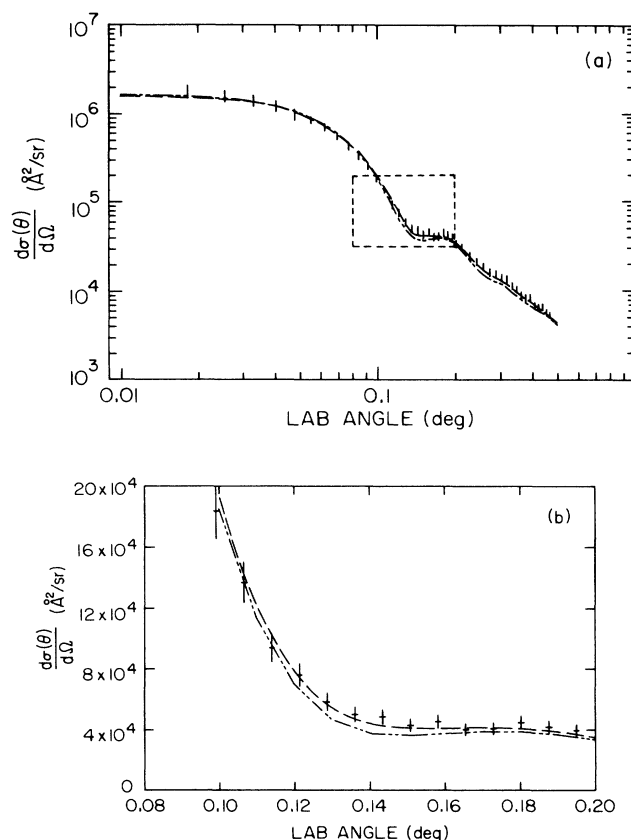


FIG. 4. (a) Comparison of experimental and theoretical differential cross sections at a projectile energy of 0.5 keV. Potentials used for the theoretical cross sections: — · — · —, Aziz *et al.* (Ref. 17); and — — —, Ceperley and Partridge (Ref. 18). (b) Enlarged view of the region between 0.08° and 0.2°.

0.2° than do the data, but are otherwise in excellent agreement with the experimental results. Our data are thus consistent with the less steeply rising of the He-He potentials in Fig. 3.

Since the structure in the data occurs over a range of angles which is large in comparison with the resolution of the experiment, the finite resolution of the apparatus should not be a significant factor in the comparison of theory and experiment. To verify this quantitatively, we calculated the convolution of the theoretical cross sections with a well-characterized apparatus function which accounts for the averaging due to the discrete rings, the beam size, and the spatial distribution of PSD pulses. The predictions with averaging differ negligibly from those without.

The range of the He-He potential probed by these data can be estimated in several ways. Calculation of a classical deflection function from the 0.5-keV phase shifts indicates that the experimental scattering angles correspond to impact parameters in the range 1.2–2.0 Å. It can also be noted that the 0.5-keV partial-wave series essentially converges at $l = 1000$, which translates into an impact parameter of 2.04 Å. Finally, empirical tests show that the cross-section predictions are insensitive to the behavior of

the potential for $r > 2 \text{ \AA}$. For example, a purely repulsive exponential extrapolation of the Ceperley and Partridge potential at larger r yields calculated cross sections almost identical to those obtained from their extrapolation that follows the attractive well of Aziz *et al.*

Experimental data for the collision energies of 1.5 and 5.0 keV appear in Figs. 5 and 6, together with the partial-wave calculations based on the Ceperley and Partridge potential. The agreement between experiment and theory is generally very good except at the largest angles in the 5.0-keV data. Here the observed cross section deviates from the single-channel elastic scattering calculation. The onset of this behavior at an energy-angle product $E\theta$ of 2 keV deg is consistent with previous observations at lower energies and correspond to the opening of inelastic channels at internuclear separations of approximately 0.5 \AA .²⁰⁻²²

CONCLUSION

This experiment demonstrates the capability for the accurate measurement of differential cross sections for fast-beam scattering at very small angles. The technique should be a fruitful one for probing the long-range interaction potentials in a wide variety of atomic and molecular systems.

ACKNOWLEDGMENTS

The authors wish to acknowledge productive discussions with J. H. Newman, N. F. Lane, and S. Estreicher, and assistance in the initial data taking by C. Chitnis. This work was supported by Welch Foundation Grant No. C-552, by National Science Foundation Grant No. ATM-8411853, and by Saint Olaf College.

APPENDIX: PARTIAL-WAVE PHASE-SHIFT CALCULATIONS

Phase shifts needed for the evaluation of Eq. (2) were obtained using the semiclassical JWKB approximation in the form

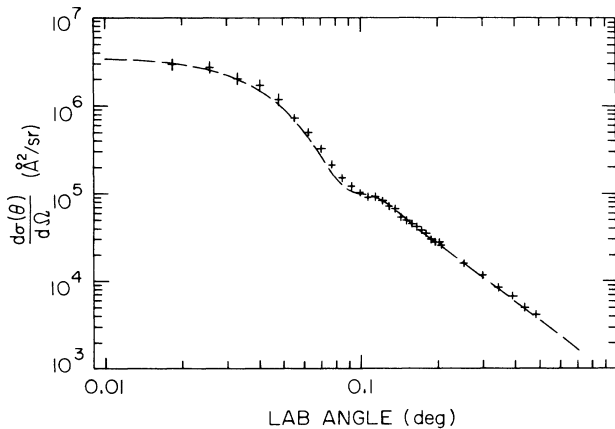


FIG. 5. Differential cross sections at a projectile energy of 1.5 keV. +, experimental results; --- theoretical prediction using the potential of Ref. 19.

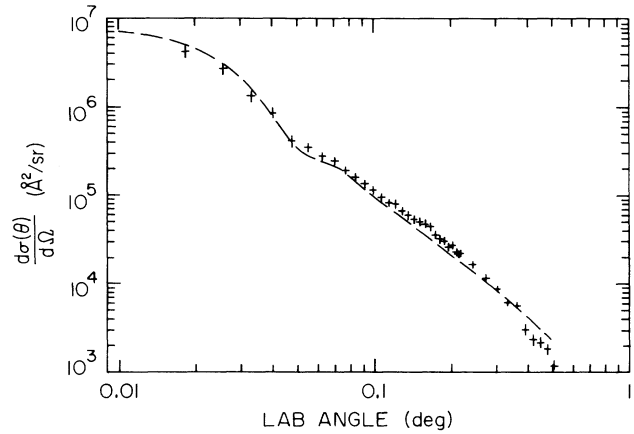


FIG. 6. Differential cross sections at a projectile energy of 5.0 keV. +, experimental results; ---, theoretical prediction using the potential of Ref. 19.

$$\delta_l^{\text{JWKB}} = kb(\pi/2 - r_0/b + I_1), \quad (\text{A1})$$

where $b = (l + \frac{1}{2})/k$ is the classical impact parameter, r_0 is the associated turning point, and I_1 is the integral

$$I_1 = \frac{1}{b} \int_{r_0}^{\infty} \left[\left(1 - \frac{V(r)}{T} - \frac{b^2}{r^2} \right)^{1/2} - 1 \right] dr \quad (\text{A2})$$

in which T represents the center-of-mass frame collision energy. In the limit of large l the phase shifts become small and can be obtained using the Jeffreys-Born (JB) approximation²³

$$\delta_l^{\text{JB}} = \frac{-k}{2T} \int_b^{\infty} \frac{V(r)}{(1 - b^2/r^2)^{1/2}} dr \equiv \frac{-k}{2T} I_2. \quad (\text{A3})$$

I_1 was evaluated using a five-panel Gauss-Legendre quadrature of order $n = 16$ on the transformed integral

$$I_1 = \frac{-r_0}{b} \int_0^1 \frac{\left[\frac{V(r_0/z)}{T} + \left(\frac{b}{r_0} \right)^2 z^2 \right]}{\left\{ \left[1 - \left[\frac{V(r_0/z)}{T} + \left(\frac{b}{r_0} \right)^2 z^2 \right] \right]^{1/2} + 1 \right\} z^2} dz, \quad (\text{A4})$$

where $z = (r_0/r)$. Results were also obtained at $n = 8$ and $n = 24$. In all cases the $n = 16$ and $n = 24$ results were identical to five figures. As an additional independent check, we compared phase shifts obtained using Eq. (A4) with results obtained by the method of Kennedy and Smith.²⁴ Agreement for small values of l was excellent; at large l the phase shifts we obtained using (6) agreed more closely with the Jeffreys-Born results. We therefore employed our (slower) method where JWKB phase shifts were used.

The integral I_2 was cast in the form

$$I_2 = b \int_0^1 \frac{V(b/z)}{z^2(1-z^2)^{1/2}} dz, \quad (\text{A5})$$

where $z = (b/r)$, and evaluated by Gauss-Chebyshev quadratures of successively higher order (up to $n = 64$) until convergence of δ_l^{JB} to within 0.1% was obtained. The numerical method was checked by verifying that phase shifts obtained using Eq. (A5) for a screened Coulomb potential agreed with known closed-form results.¹²

Our initial procedure was to use δ_l^{JWKB} up to sufficiently large l such that δ_l^{JWKB} and δ_l^{JB} differed by less than 0.005 radians, and then use δ_l^{JB} up to a value l_{\max} equal to 2000 at 0.5 keV, 3000 at 1.5 keV, and 4000 at 5.0 keV. At

these limits the phase shifts had decreased to a magnitude smaller than 0.0005 radians and convergence of the cross sections to four significant figures was generally obtained. In practice we found that the small-angle cross sections obtained by this procedure were identical to those obtained using the Jeffreys-Born approximation for all l , confirming an assumption made by other authors in similar circumstances.^{4,5} In the results reported here, JWKB phase shifts were used for the Ceperley and Partridge potential at 0.5 and 5.0 keV. In the other cases the JB phase shifts alone were used.

*Permanent address: Physics Department, Saint Olaf College, Northfield, MN 55057.

¹J. H. Newman, K. A. Smith, R. F. Stebbings, and Y. S. Chen, *J. Geophys. Res.* **90**, 11 045 (1985).

²R. Feltgen, H. Kirst, K. A. Köhler, H. Pauly, and F. Torello, *J. Chem. Phys.* **76**, 2360 (1982).

³R. A. Aziz, in *Inert Gases*, Vol. 34 of *Springer Series in Chemical Physics*, edited by M. L. Klein (Springer-Verlag, New York, 1984), pp. 10–14.

⁴H. J. Beier, *J. Phys. B* **6**, 683 (1973).

⁵V. B. Leonas and A. V. Sermyagin, *Khim. Vys. Energ.* **11**, 296 (1977) (in Russian).

⁶R. S. Gao, P. S. Gibner, J. H. Newman, K. A. Smith, and R. F. Stebbings, *Rev. Sci. Instrum.* **55**, 1756 (1984).

⁷H. J. Blaauw, R. W. Wagenaar, D. H. Barends, and F. J. de Heer, *J. Phys. B* **13**, 359 (1980).

⁸E. A. Mason, J. T. Vanderslice, and C. J. G. Raw, *J. Chem. Phys.* **40**, 2153 (1964).

⁹R. J. Munn, E. A. Mason, and F. J. Smith, *J. Chem. Phys.* **41**, 3978 (1964).

¹⁰F. J. Smith, E. A. Mason, and J. T. Vanderslice, *J. Chem. Phys.* **42**, 3257 (1965).

¹¹M. V. Berry, *J. Phys. B* **2**, 381 (1969).

¹²K. E. Mount, *J. Phys. B* **6**, 1397 (1973).

¹³H. J. Beier, *J. Phys. B* **6**, 2564 (1973).

¹⁴See footnotes 1–17 of Ref. 2.

¹⁵See footnote 48 of Ref. 2.

¹⁶P. B. Foreman, P. K. Rol, and K. P. Coffin, *J. Chem. Phys.* **61**, 1658 (1974).

¹⁷R. A. Aziz, V. P. S. Nain, J. S. Carley, W. L. Taylor, and G. T. McConville, *J. Chem. Phys.* **70**, 4330 (1979).

¹⁸D. M. Ceperley and H. Partridge, *J. Chem. Phys.* **84**, 820 (1986).

¹⁹B. J. Jody, S. C. Saxena, V. P. S. Nain, and R. A. Aziz, *Chem. Phys.* **22**, 53 (1977).

²⁰R. Morgenstern, M. Barat, and D. C. Lorents, *J. Phys. B* **6**, L330 (1973).

²¹J. C. Brenot, D. Dhuicq, J. P. Gauyacq, J. Pommier, V. Sidis, M. Barat, and E. Pollack, *Phys. Rev. A* **11**, 1245 (1975).

²²J. P. Gauyacq, *J. Phys. B* **9**, 2289 (1976).

²³H. S. W. Massey and C. B. O. Mohr, *Proc. R. Soc. London, Ser. A* **144**, 188 (1934).

²⁴M. Kennedy and F. J. Smith, *Mol. Phys.* **13**, 443 (1967).